Limb observations of the ultraviolet nitric oxide nightglow with SPICAV on board Venus Express

J.-C. Gérard,[1] C. Cox,[1] A. Saglam,[1] J.-L. Bertaux,[2] E. Villard,[2] and C. Nehmé[2]

Received 17 January 2008; revised 15 April 2008; accepted 30 May 2008; published 20 August 2008.

[1] Limb observations of the spectrum of nightglow emission in the δ (190–240 nm) and γ (225–270 nm) bands of nitric oxide have been made with the Spectroscopy for Investigation of Characteristics of the Atmosphere of Venus (SPICAV) ultraviolet spectrometer on board Venus Express. These emissions arise from radiative recombination between O(^{3}P) and N(^{4}S) atoms that are produced on the dayside and recombine to form excited NO molecules on the nightside. No other emission feature has been identified. The mean altitude of the emission layer is located at 113 km, but it varies between 95 and 132 km. The mean brightness of the total NO emission at the limb is 32 kR, but it is highly variable with limb intensities as large as 440 kR observed at low latitude and values below 5 kR seen at northern midlatitudes. No systematic dependence of the brightness with latitude is observed, but the mean altitude of the emission maximum statistically drops with increasing latitude between 6° and 72°N. Typical observed limb profiles are compared with simulations based on a one-dimensional chemical-diffusive atmospheric model. From model fits to observed profiles, we find that the downward flux of N atoms at 130 km typically varies between 1×10^8 to 4×10^9 atoms cm^{-2} s^{-1}. Comparisons of observed airglow topside scale heights with modeled profiles smoothed by the instrumental field of view indicate that the observations are compatible with a downward flow of O and N atoms by molecular and turbulent transport above the peak of emission. The K coefficient deduced from comparisons to limb profiles is less than that determined from the observations made with the Pioneer Venus UV spectrometer at low latitude during periods of high solar activity.

Citation: Gérard, J.-C., C. Cox, A. Saglam, J.-L. Bertaux, E. Villard, and C. Nehmé (2008), Limb observations of the ultraviolet nitric oxide nightglow with SPICAV on board Venus Express, *J. Geophys. Res.*, *113*, E00B03, doi:10.1029/2008JE003078.

1. Introduction

[2] The presence of the delta and gamma bands of nitric oxide in the Venus nightglow was detected and identified by *Feldman et al.* [1979] using the ultraviolet spectrograph on board the International Ultraviolet Explorer (IUE). It was also observed by *Stewart and Barth* [1979] in spectra obtained with the ultraviolet spectrometer on board the Pioneer Venus Orbiter (PV-OUVS). The emission process is radiative recombination through reverse predissociation of nitrogen N(^{4}S) and oxygen O(^{3}P) atoms, yielding excited NO* molecules which emit the ultraviolet δ and γ bands:

$$\mathrm{N} + \mathrm{O} \rightarrow \mathrm{NO}\left(\mathrm{C}^2\Pi\right) \quad (1)$$

giving rise to

$$\mathrm{NO}\left(\mathrm{C}^2\Pi\right) \rightarrow \mathrm{NO}\left(\mathrm{X}^2\Pi\right) + \delta\text{-bands},$$

or

$$\mathrm{NO}\left(\mathrm{C}^2\Pi\right) \rightarrow \mathrm{NO}\left(\mathrm{A}^2\Sigma, \mathrm{v}' = 0\right) + 1.22\,\mu\mathrm{m},$$

followed by

$$\mathrm{NO}\left(\mathrm{A}^2\Sigma, \mathrm{v}' = 0\right) \rightarrow \mathrm{NO}\left(\mathrm{X}^2\Pi\right) + \gamma\text{-bands}$$

[3] As a consequence, the total emission rate of the NO bands is proportional to the rate of recombination of O and N atoms and thus depends on the nitrogen and oxygen densities. A detailed study of reaction (1) [*Dalgarno et al.*, 1992] suggests a rate coefficient for the N + O recombination equal to $1.92 \times 10^{-17} \times (300/\mathrm{T})^{1/2} \times (1-0.57/\mathrm{T}^{1/2})$ cm^3 s^{-1}. The N and O atoms are produced by dissociation of N_2, CO_2 and CO on the dayside.

[4] Spin-scan images in the wavelength of the δ (0,1) band at 198 nm obtained from Pioneer Venus near apoapsis by *Stewart et al.* [1980] indicated important day-to-day variations. Patches of enhanced intensity appeared to vary in intensity and location without correlation with solar activity. The location of the brightest spots ranged from 2130 to 0300 LT and 39°S to 60°N. This variability was attributed to temporal charges in the Venus thermospheric circulation on

[1] Laboratoire de Physique Atmosphérique et Planétaire, Université de Liège, Liège, Belgium.
[2] Service d'Aéronomie du CNRS, Université Versailles Saint Quentin, Verrières-le-Buisson, France.

0148-0227/08/2008JE003078

timescales of one Earth day or less. It appears to be caused by instabilities in the large-scale circulation, possibly as a result of wind shears near the terminator or time-varying wave drag from gravity waves. However, no quantitative modeling for this variability has been made so far. *Stewart et al.* [1980] also showed that, statistically, the emission is concentrated in a bright spot located near 0200 local solar time, just south of the equator. Following revision of the calibration of the instrument [*Bougher et al.*, 1990], the emission rate of this region was estimated to ~1.9 kR. From these observations, a general picture emerged where production of O and N atoms by solar EUV and possible solar particle impact occurs on the dayside, followed by global transport to the nightside, downward transport and radiative recombination. It was found that parameters such as the downward flux of O and N atoms and the strength of turbulent transport in a one-dimensional model could be adjusted to reproduce the average NO nightglow intensity. Since the attitude of the spacecraft was not known with sufficient accuracy, the determination of the altitude of the emission peak was indirect and based on the absorption of the NO emission by CO_2. *Gérard et al.* [1981] observed that it lies close to 115 km. They showed that downward transport by molecular diffusion alone is not sufficient to reproduce the observations. They parameterized turbulent mixing using an eddy diffusion coefficient $K \sim 8 \times 10^{12}/n^{1/2}$ cm^2 s^{-1}, where n is the total number density. This value was close to that deduced by *von Zahn et al.* [1979] from the analysis of the neutral composition measured near the morning terminator, which sets the altitude of the homopause close to 135 km.

[5] Globally, the general picture of production of O and N atoms followed by transport to the nightside by the subsolar to antisolar circulation, downward turbulent mixing and radiative recombination appeared quantitatively consistent with the PV-OUVS observations. Further quantitative validation of this scheme was obtained by three-dimensional simulations using the Venus Thermospheric General Circulation Model (VTGCM) [*Bougher et al.*, 1990]. One-dimensional chemical-transport calculations of odd nitrogen species on the dayside indicated that the daytime N average production is $\sim 1.3 \times 10^{10}$ atoms cm^{-2} s^{-1} for solar maximum activity (F10.7 = 180–200) [*Gérard et al.*, 1981]. Parameter adjustments in the VTGCM lead to an average production of about 9×10^9 atoms cm^{-2} s^{-1}, approximately 30% of which are needed for transport to the nightside to reproduce the observed average nightglow brightness. The statistical location of the bright spot was also reasonably well reproduced by the 3-D model and implied zonal winds of about 50–75 m s^{-1} in the 115–150 km region. However, it was found that model parameters could be adjusted to reproduce either the ultraviolet nightglow or the observed N density on the dayside but not both. Predictions for solar minimum conditions indicated a reduction by a factor of ~3 from solar maximum. This is a direct consequence of the lower production of N and O atoms on the dayside and of the predicted reduced strength of the thermospheric circulation. The observed shift toward dawn of the statistical location of the airglow maximum, presumably as a consequence of the residual atmospheric superotation in the upper mesosphere, was reproduced by the VTGCM.

[6] The NO δ and γ bands were also detected on Mars by *Bertaux et al.* [2005] using the SPICAM (Spectroscopy for Investigation of Characteristics of the Atmosphere of Mars) spectrometer on board the Mars Express spacecraft. The distribution and variability of the NO Mars airglow were recently described by *Cox et al.* [2008]. They found that the peak of the airglow layer is located between 55 and 92 km with lower values observed at higher latitude and larger values at low latitudes and midlatitudes. The limb brightness was also found to be very variable, ranging from less than 0.2 to 10.5 kR with the large values occurring at southern latitudes higher than 50°.

[7] The NO airglow is thus a tracer of the thermospheric circulation and its distribution and intensity provide constraints on transport models in a region of the Venusian atmosphere difficult to probe with other in situ or remote sensing methods [*Bougher et al.*, 2006]. In this study, we describe new observations of the NO nightglow collected in the northern hemisphere with the Spectroscopy for Investigation of Characteristics of the Atmosphere of Venus (SPICAV) spectrometer on board the Venus Express spacecraft [*Svedhem et al.*, 2007]. In particular, we investigate the distribution of the altitude and brightness of the airglow and its spatial variability. We examine possible relationships between the emission intensity and its brightness and a possible latitudinal dependence. We also compare limb profiles with results of a one-dimensional chemical-diffusive model solving the odd nitrogen and oxygen continuity equations and draw conclusions concerning the importance of transport by other processes.

2. SPICAV Observations

[8] The observations described in this study were obtained with SPICAV, the ultraviolet and infrared spectrometer on board Venus Express. The instrument and its performances were described by *Bertaux et al.* [2007a]. The ultraviolet component covers the range extending from 118 nm to 320 nm and includes the NO δ ($C\ ^2\Pi$ - $X\ ^2\Pi$) and γ ($A\ ^2\Sigma$ - $X\ ^2\Pi$) emission bands. For reasons of telemetry limitations but also because of the time needed to read all the lines of the CCD, only 5 adjacent zones of the CCD detector are usually read out. Each zone (or spatial bin) is made of 1, 2, 4, 8, 16 or 32 lines of the CCD following a preselected mode. Therefore each spatial bin covers a different region of the atmosphere separated by an angle ranging from 1.4 to 22.4 arcmin, depending on the spatial binning. In the case of the NO airglow limb scans reported here, each spatial bin includes 2, 4, 8, 16 or 32 adjacent pixel lines. These lines are seen through the large (500 μm) or the small (50 μm) slits, which provides a spectral resolution of 12 or 1.5 nm, respectively. The SPICAV CCD is read every second and therefore five spatial bins corresponding to five adjacent portions of the SPICAV field of view are recorded each second. In each individual spectrum non-uniform dark current and offset values are subtracted. Finally, the intensities are calibrated in kiloRayleighs (kR) using well-known hot stars spectra observed by SPICAV during the mission.

[9] The VEX spacecraft moves along a quasi-polar eccentric orbit with a 24-hour period. The pericenter and apocenter are located at 250 km and 66,000 km,

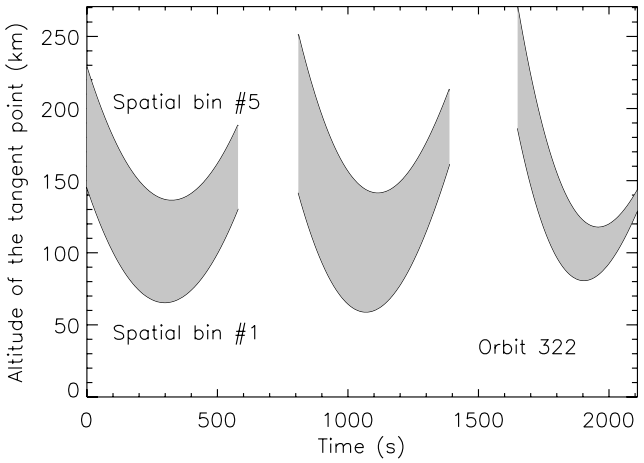

Figure 1. Variation of the altitude of the tangent point of the center of the field of view for SPICAV spatial bins 1 and 5 during tangential limb nightside observations of orbit 322. The altitudes of the other three spatial bins are within the gray shaded area.

respectively, and the orbit precesses in local time at the rate of 1.6°/day. The precession of the orbital plane leads to a wide variety of configurations on the nightside as well as on the dayside. Several observation modes ("science cases") may be selected including nadir observations, star pointing for stellar occultations by Venus' atmosphere, fixed point tracking and limb observations [*Titov et al.*, 2006]. A particular mode is well suited for high spatial resolution airglow observations. In this grazing (tangential) limb mode, the line of sight is at some angle to the orbital plane and moves in such a way to maximize the time spent in the atmosphere, so that the time of observation of the limb is larger than in the usual limb mode in the orbital plane [*Bertaux et al.*, 2007a]. The signal recorded by the CCD detector is integrated over 640 ms periods typically during about 10 min. In this way, the line of sight scans a range of altitudes, generally between 70 km and 400 km and each second a full UV spectrum is obtained. For most of the observations reported here, the spacecraft was oriented in such a way that the SPICAV line of sight scanned the dark limb several times during the ascending portion of the VEX orbit. Since the line of sight crossed the same altitudes once during the ingress and once during the egress segments owing to the geometry of the grazing limb observation type, SPICAV supplied several sets of two (one for ingress, one for egress) altitude scans of five (for the 5 spatial bins) altitude profiles at each orbit. Consequently, as many as 6 × 5 limb profiles of the NO airglow were obtained on a same orbit between 6.1° and 71.8°N. At this date, a total of 17 orbits and 201 limb scans with suitable night airglow observations have been collected. As an example, Figure 1 shows the altitude variation of the altitude of the tangent point of the central point of the field of view for SPICAV spatial bins 1 and 5 during orbit 322. Other spatial bins scan the region indicated by the dotted gray area. Once all profiles are retrieved, the finite aperture of the field of view projected onto the limb is taken into account. For a given airglow layer, the apparent altitude of the emission peak and the maximum brightness depend on the value of the field of view projected on the limb. The angular field of view of one pixel is equal to 0.7 arcmin and the bin parameter varies between 2 and 32. The distance between the spacecraft and the observed tangent point lies within the 3000 to 12000 km range and the angle between the SPICAV slit and the limb is between 15° and 72°. For each observation, this set of parameters is used to determine the field of view projected on the limb. It varies from 3 to 27 km, but generally remains between 12 and 22 km, with a mean value of 14.9 km. We have investigated the effects of the smoothing by the field of view of an emission layer having a vertical Chapman profile integrated along the line of sight. Each Chapman profile is constrained to show the same topside scale height as the observation. It is found that the peak intensity observed by SPICAV decreases by a factor between 1 and 2 and the altitude of the peak is slightly above the unconvolved value. Data points in Figures 6 to 10 have been corrected for this smoothing effect by setting the peak intensity and altitude to the values they would have if the limb profiles had been observed with a negligibly small field of view.

[10] For this study, we have integrated each spectrum over the entire δ and γ bands emission between 190 nm and 260 nm, including both the δ and the γ bands. As discussed in section 1, the total emission rate of the two molecular systems is equal to the N + O recombination rate. Figure 2 shows a sum of all (771) individual nightglow spectra obtained between 90 and 120 km on orbit 516. Comparison with the laboratory spectrum of the N(^{4}S) + O(^{3}P) recombination [*Groth et al.*, 1971] confirms that this region of the Venus nightglow ultraviolet spectrum contains no other emission than those arising from the C $^2\Pi$ and A $^2\Sigma$ states of NO. Integration of each individual spectrum over this spectral domain provides the total NO emission brightness in kR for each scanned altitude. Figure 3 shows limb profiles of the NO nightglow measured on ingress and egress segments of randomly selected orbit 271. In this plot, since the limb profiles in the five spatial bins are very similar as it is generally the case, the data points for spatial elements 1 and 2 have been grouped together. The data points were first binned in altitude (in 2 km steps), and these binned profiles were then co-added, separating egress and ingress data. Depending on altitude, each bin contains between 10 and 20 spectra, so that the error bar are quite small. The latitudes of the peak emission at ingress and egress are 21.7°N and 29.7°N and the local times are 2348 and 2330 LT, respectively. The maximum intensities at the peak are 46 and 35 kR, indicating the presence of a substantial gradient over a distance of only 8.0 degrees of latitude. The limb intensities have been numerically inverted using an Abel algorithm assuming a horizontally homogeneous distribution to calculate the corresponding vertical emission rates of 0.8 and 0.9 kR. These values may be compared with the 1.9 kR statistically observed by PV-OUVS brightness in the bright spot. As just mentioned the limb profiles observed in the spatial bins are generally close to each other. However, strong horizontal gradients are occasionally present and noticeable differences between the profiles in the spatial bins may then be observed. An example is given in Figure 4 which shows four ingress smoothed profiles obtained during VEX orbit 322. The line of sight for spatial bin 5 did not intersect the altitude of the

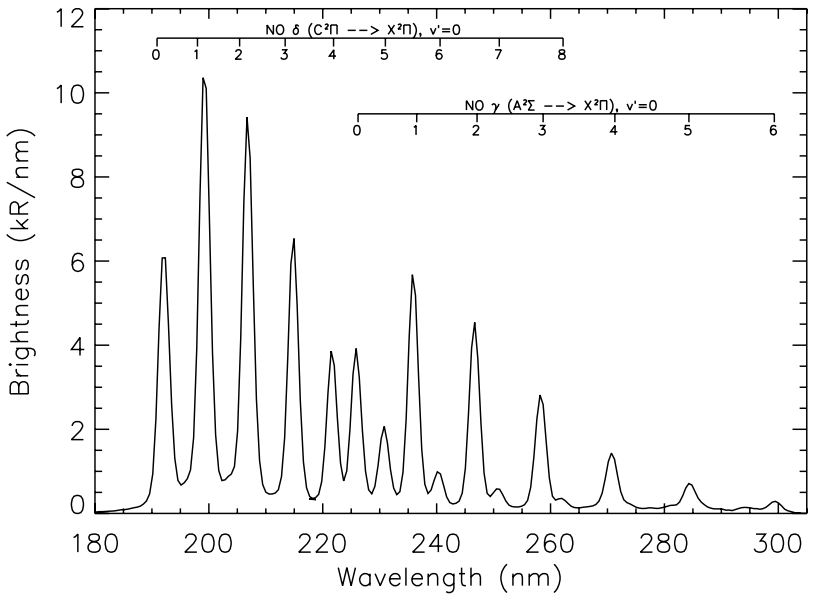

Figure 2. Spectrum of the nitric oxide ultraviolet nightglow obtained by summing all 771 individual spectra collected with the SPICAV instrument between 90 and 120 km on VEX orbit 516.

maximum of the airglow layer and is thus not represented in Figure 4. Moving from spatial bin 1 to 4, the limb intensity first increases then drops between adjacent bins angularly separated by only 5.6 arcmin. This separation maps into 1.8 (between bin 1 and 2), 1.4 (between bin 2 and 3) and 3.5 (between bin 3 and 4) degrees of increasing planetary latitude at the emission peak, which corresponds to 197, 158, and 374 km, respectively, of horizontal distance of the tangent points along the line of sight. Similarly, the altitude of the airglow peak varies from a bin to the next one. The differences in shape, peak altitude and brightness observed in the 4 spatial bins indicate that, in this case, the NO airglow distribution is significantly non uniform even over a restricted range of latitudes. It is important to note, however, that latitudinal gradients are usually much smaller, as was shown for example in Figure 3.

[11] Each observed limb profile can be characterized by the altitude, brightness, latitude and local time of the maximum emission brightness. We first apply a filter to each limb profile to remove some of the high spatial frequency fluctuations through the data point following noise and background subtraction. From these fits we determine the peak altitude, the topside scale height of the emission as well as the total NO peak brightness. In this data set, covering the period between 17 January and 19 September 2007, a total of 201 good quality limb profiles were obtained. Their local time covers the range from 2000 to 0300 LT. The local time and latitudinal distribution of the observed limb profiles included in the database is represented in Figure 5. It shows that most observations were collected in two separate groups. Group 1 includes profiles between 6.1°N and 71.8°N observed in the post-midnight sector (2400 to 0300 LT), while group 2 which is more widespread corresponds to midlatitude to low-latitude observations between 2000 and 2200 LT. It should be noted that no observations were made in the region of the NO bright spot observed with PV-OUVS south of the equator in the post-midnight period.

3. Correlations

[12] We first examine the statistical distribution of the altitude of the peak of the airglow emission, corrected for the smoothing effect of the finite field of view. Figure 6 shows the distribution, where the data points have been distributed into 2.5 km altitude bins. The distribution is

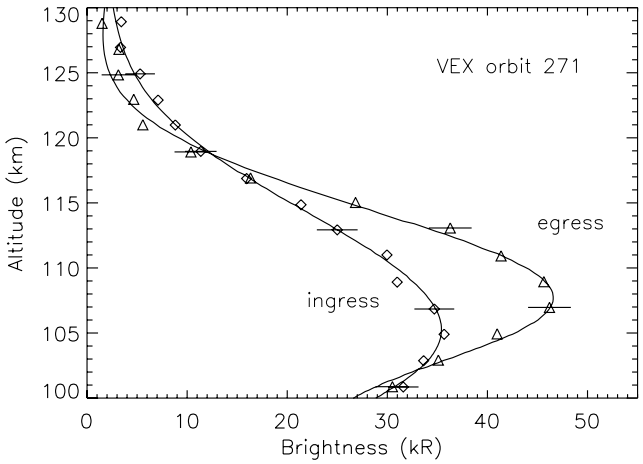

Figure 3. Limb profile of the NO airglow measured on the ingress and egress of VEX orbit 271 on 17 January 2007. The latitudes of the peak emission are 21.7°N and 29.7°N and local times 2348 LT and 2330 LT for ingress and egress, respectively. The raw data are represented by open triangles and diamonds, while the smooth profile is obtained following Fourier filtering of high spatial frequencies. The error bars include the effect of the photon statistics and the detector thermal noise.

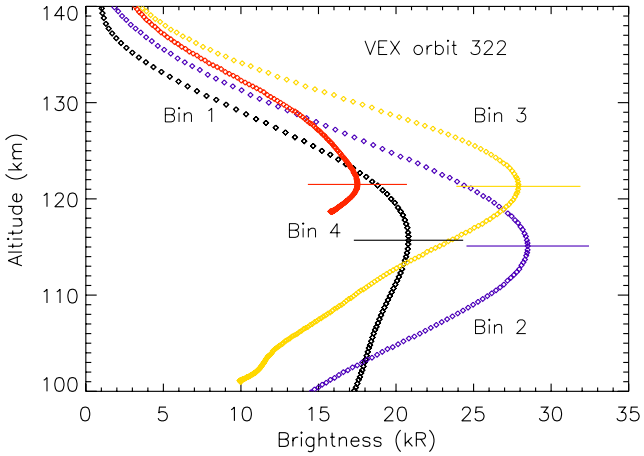

Figure 4. Smoothed limb profiles observed during ingress of the line of sight during VEX orbit 327 in four adjacent spatial bins on the CCD detector. The error bars include the effect of the photon statistics and the detector thermal noise.

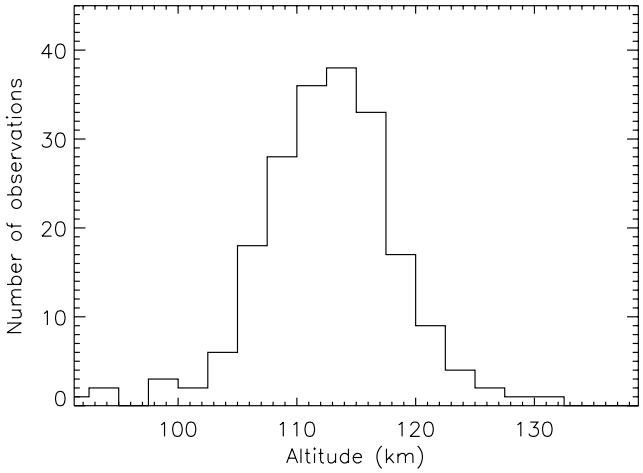

Figure 6. Distribution of the altitudes of the tangent points corresponding to the peak in the airglow limb profiles analyzed in this study. The altitudes have been corrected to account for the smoothing effect of the SPICAV field of view (see text).

quite symmetric about the mean value, with some values above 125 km and a few profiles with a peak below 100 km. The mean value is 112.6 km, quite close to the median value of 112.9 km, with a 1-σ deviation of 5.8 km. It should be noted that we implicitly assume a horizontal homogeneous layer. If the emission is not present (or weaker) at the limb but present (or stronger) in the foreground or in the background behind the limb, then the derived altitude of the peak is necessarily lower than the actual altitude. Therefore, this effect cannot explain the high-altitude peaks which are shown in Figure 6.

[13] The distribution of the peak brightness with a 6 kR bin size is shown in Figure 7. It is much less symmetric, showing an extended tail of high-intensity values. The mean limb total NO brightness is 32 kR and the median value is 19 kR, with a standard deviation of 60 kR. The large emission rate of 440 kR observed at the limb on VEX orbit 516 (19 September 2007) has not been included in this nor in the following plots for reasons of graphical representations. The large scatter suggests that the large-scale winds which carry the O and N atoms from the dayside are intrinsically variable. As the wind pattern and velocity change, the amount of atoms transported to a given location and the position of the subsidence region considerably fluctuate, generating variability of the bright airglow spot location and intensity.

[14] We now search for possible correlations between the altitude of the airglow, its brightness and latitude. Figure 8 shows the altitude of the airglow peaks plotted versus its latitude between 11° and 85°N. A slow decrease is observed toward the polar region as indicated by the linear regression obtained by minimizing the chi-squares, which shows a drop of about 5 km from low to high latitude. However, the linear correlation coefficient is equal to only −0.26. Figure 9 shows the lack of correlation (r = −0.19) between the

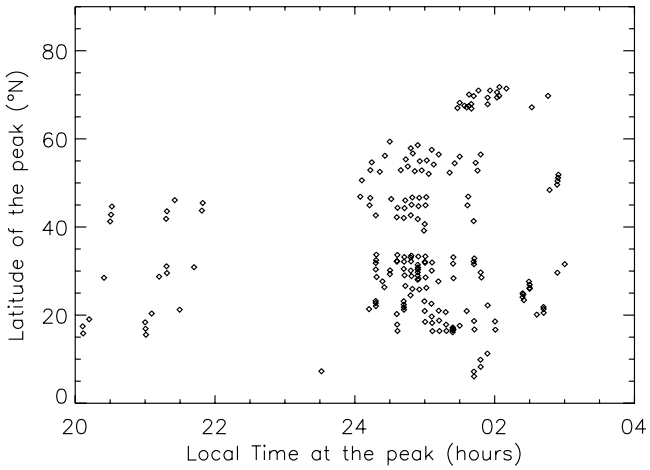

Figure 5. Local time and latitudinal coverage of the limb profiles used in the statistical study of the NO airglow distribution.

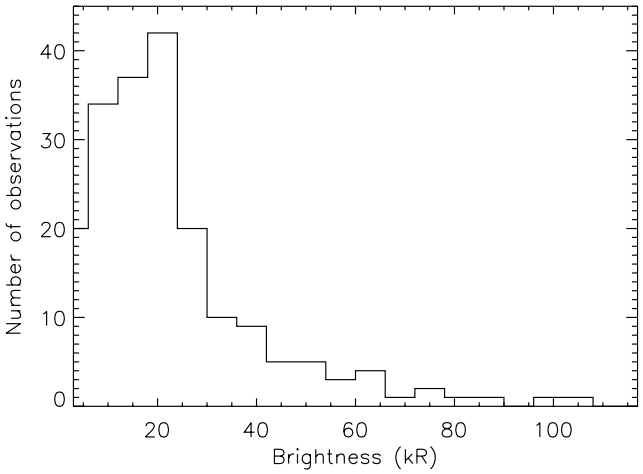

Figure 7. Distribution of the brightness of the peaks in the airglow limb profiles analyzed in this study. The intensities have been corrected to account for the smoothing effect of the SPICAV field of view.

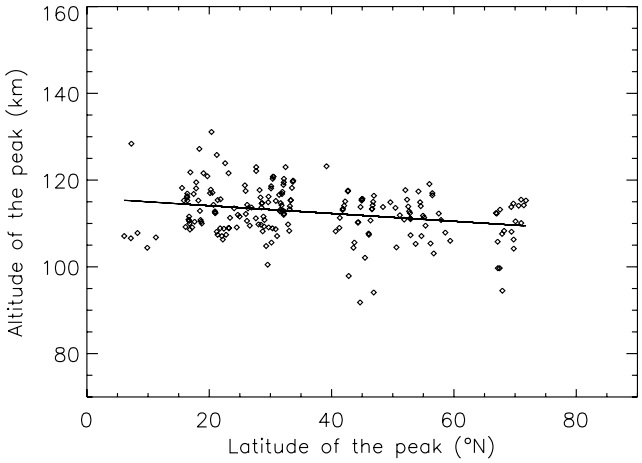

Figure 8. Relationship between the altitude of the tangent point of the emission peak and its latitude.

airglow peak intensity and the latitude of the tangent point. However, the largest intensities are observed at latitudes between 20° and 50°N and 65° and 70°N. It should be noted that the large values between 65° and 70° are located far from the statistical bright spot observed with PV-OUVS. Figure 10 illustrates how these brightness data points are distributed with the altitude of the airglow peak. Although a considerable scatter is observed (r = −016), it appears that the large intensity limb profiles are generally concurrent with a peak altitude located in the vicinity of 113 ± 4 km, close to the mean altitude of the airglow layer. By contrast, profiles showing weaker emission rate correspond to situations where the peak altitude is outside this range of central values.

4. One-Dimensional Modeling

[15] The use of a one-dimensional model makes it possible to evaluate the downward flux of nitrogen and oxygen atoms that recombine to produce the NO airglow emission. As described in the introduction, the current global view is that the subsolar to antisolar (SSAS) circulation carries atoms from the day to the night side, where the combination of the global circulation and local turbulent transport carries the atoms in the region where they recombine near 115 km. The one-dimensional model developed for this study brings into play diffusion equations as well as production and loss by chemical reactions. It is similar to that described by *Cox et al.* [2008] to model the NO nightglow on Mars. The continuity equation for a minor constituent i in the thermosphere may be written

$$\frac{\partial n_i}{\partial t} = -\frac{\partial \phi_i}{\partial z} + P_i - L_i - \frac{\partial (n_i w)}{\partial z} \tag{2}$$

with the vertical diffusive flux ϕ_i of a minor constituent i given by

$$\phi_i = -(D_i + K)\left(\frac{\partial n_i}{\partial z} + \frac{n_i}{T}\frac{\partial T}{\partial z}\right) - \left(\frac{D_i}{H_i} + \frac{K}{H}\right) n_i \tag{3}$$

with D_i the molecular diffusion coefficient for constituent i, K is the vertical eddy diffusion coefficient, H_i is the local scale height of the ith constituent. H is the atmospheric scale height, T is the neutral gas temperature, n_i is the number density of the ith species, z is the altitude, t is time, P_i is the production rate of species i, L_i the loss rate and w is the vertical velocity positive upward. The last term in equation (2) corresponds to the vertical advective flux. We adopt the vertical variation of the eddy diffusion coefficient K similar to that used in earlier studies [*von Zahn et al.*, 1979; *Gérard et al.*, 1981], that is,

$$K(z) = \frac{A}{\sqrt{n(z)}} \mathrm{cm}^2\ \mathrm{s}^{-1} \tag{4}$$

where n is the total number density and A is a free parameter of the model which is independent of altitude. Therefore, K only depends on altitude and is identical for all constituents. The model solves equation (2) for $O(^3P)$, $N(^4S)$, NO and O_2 ($^1\Delta$). The P_i and L_i coefficients depend on the choice of the different reactions that come into play and which are listed in Table 1 with their corresponding reaction coefficients. The temperature dependence of the

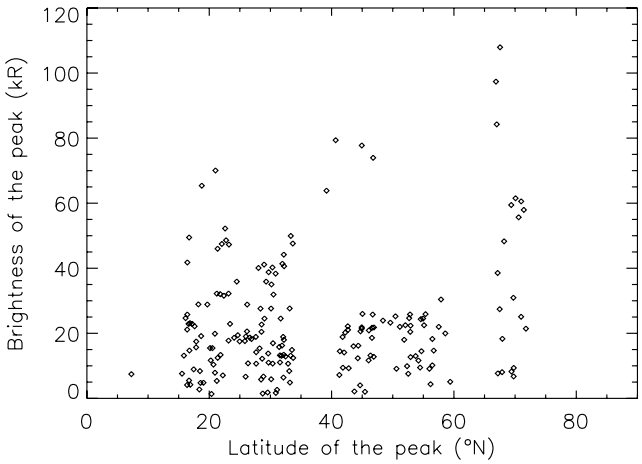

Figure 9. Relationship between the brightness of the emission peak and its latitude.

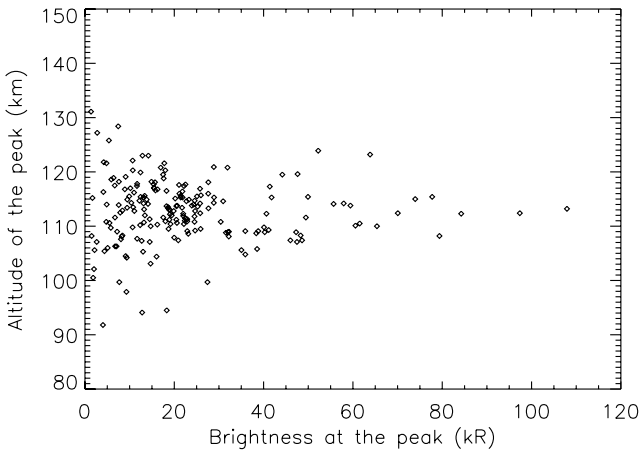

Figure 10. Relationship between the tangent point altitude of the emission peak and its brightness.

Table 1. Chemical Reactions and Rate Coefficients

Reaction	Rate Coefficient[a] ($cm^3\ s^{-1}$)	Reference
(R1) $N + O \rightarrow NO + hv$	$1.9 \times 10^{-17} \times (300/T)^{1/2} \times (1-0.57/T^{1/2})$	*Dalgarno et al.* [1992]
(R2) $N + O + CO_2 \rightarrow NO + CO_2$	$2.8 \times 10^{-32}\ (300/T)^{1/2}$	*Campbell and Thrush* [1966][b]
(R3) $N + NO \rightarrow N_2 + O$	$2.5 \times 10^{-10} \times (T/300)^{1/2} \times \exp(-600/T)$	*Fox* [1994]
(R4) $O + O + CO_2 \rightarrow O_2 + CO_2$	2.8×10^{-32}	*Campbell and Gray* [1973][c]

[a]Except for three-body recombination reactions (R2) and (R4) in $cm^6\ s^{-1}$.
[b]The rate coefficient of (R2) is the value measured with $M = N_2$ as a third body, multiplied by 2.5 for $M = CO_2$ with an inverse square root dependence on temperature.
[c]The rate coefficient is the value measured for $M = N_2$ at 196 K multiplied by 2.5, a factor recommended as appropriate for Mars atmosphere models [*Nair et al.*, 1994].

$N + O + CO_2$ reaction was introduced by *Stewart et al.* [1980] and used in subsequent models such as *Yung and DeMore* [1982]. For reasons of continuity, we have adopted the same temperature dependence as earlier studies. Equation (2) is solved numerically between 130 and 80 km using the finite volume method on a constant grid. For O and N, we apply a flux boundary condition through the upper boundary, and assume photochemical equilibrium at the lower boundary and we use density null vectors for initial conditions (except at the boundaries). The model is then parameterized by A, w(z), Φ_o and Φ_N. In fact, the choice of the densities at 80 km is relatively arbitrary and it does not influence the solution further than one scale height from the lower boundary if it is kept in a reasonable range. At the upper boundary, we leave the $O(^3P)$ and the $N(^4S)$ fluxes as free parameters to be determined by fitting the modeled limb profile to the observations. The limb profile of the nitric oxide emission is obtained by integrating the k[O][N] product along the line of sight, where k is the rate coefficient of the O + N recombination. We note that in all limb profiles most of the emission is located below 135 km, the altitude of the homopause determined from the composition measurements made by the Pioneer Venus large probe during its descent [*von Zahn et al.*, 1979]. One-dimensional models usually do not include advection terms. Consequently, in this representation, vertical transport is solely the result of the molecular and eddy diffusions, and advection is implicitly contained in the K coefficient, despite the lack of physical meaning.

[16] We first present results of modeled limb profiles using CO_2 density and temperature taken from the Venus Reference Atmosphere (VIRA) model in the code formulation given by *Hedin et al.* [1983]. Figure 11 shows a comparison between three observed limb profiles and those simulated using the one-dimensional model described above, following integration of the calculated volume emission rate along the line of sight. Absorption of the NO bands by CO_2 is less than 1% in the altitude region considered here and is thus negligible. The simulated distributions match reasonably well the peaks of the observed limb profiles. As in earlier studies [*Stewart et al.*, 1980; *Gérard et al.*, 1981], we have assumed that the flux of $N(^4S)$ is 1% of the O flux, in agreement with the average O/N number density ratio measured in the dayside thermosphere with the neutral mass spectrometer on board Pioneer Venus. The observational data have been smoothed as described in section 2 to remove most of the scatter associated with instrument noise. In Figure 11, three comparisons are made with profiles that have been selected to cover a range of altitudes of the emission peak. The profile for orbit 320 obtained on 7 March 2007 at 32.3°N and 0036 LT shows a maximum at 112 km and is typical of a vertical distribution frequently observed. The peak intensity reaches 39 kR, a value larger than the median but close to

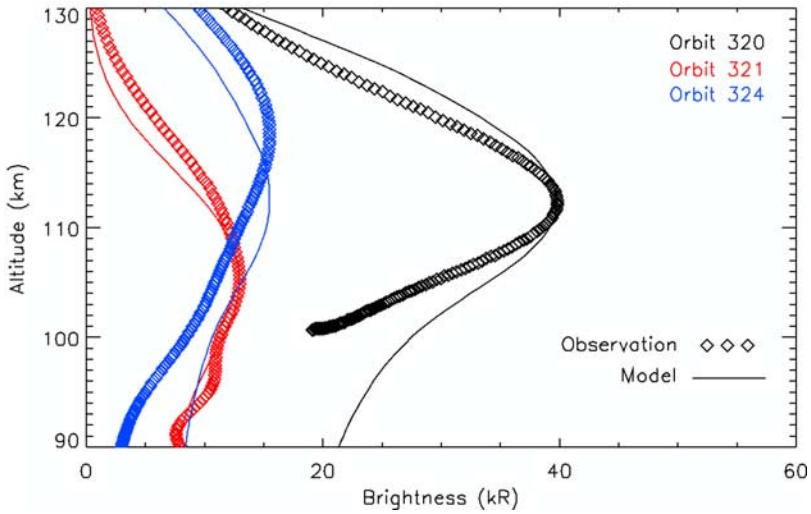

Figure 11. Examples of airglow limb profiles with different peak altitudes (circles). The solid lines show the corresponding model simulations that best fit the altitude and brightness of the airglow maximum.

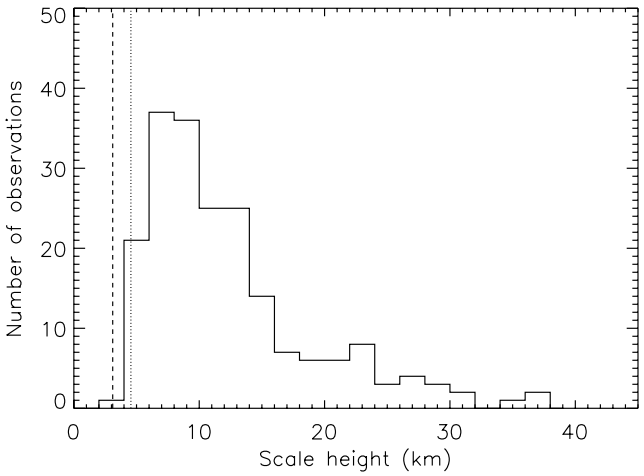

Figure 12. Distribution of the apparent topside scale heights of the airglow limb profiles in the region located above the emission peak. For comparison, the dotted line indicates the airglow scale height for diffusive equilibrium of O and N, while the dashed line is the expected value for a downward flow of atoms in the homosphere (see text).

the mean value, as was shown in Figure 7. The calculated limb profile represented by the solid line was obtained using the CO_2 density and temperatures profiles from the Venus Reference Atmosphere (VIRA) model in the code formulation given by *Hedin et al.* [1983], for the appropriate latitude, local time and solar activity level. The calculated limb profile has been convolved by the value of the field of view projection on the planet calculated for the pixel binning and the spacecraft-Venus distance at the time of the observation. The parameters used for this simulation were $\Phi_O = 2.1 \times 10^{11}$ cm^{-2} s^{-1}, $\Phi_N = 2.1 \times 10^9$ cm^{-2} s^{-1}, $A = 7.4 \times 10^{11}$. The altitude distribution at the peak and the topside scale height are well reproduced by the model, whereas the calculated bottomside scale heights are somewhat larger than the observed values. *Bertaux et al.* [2007b] showed that SPICAV stellar occultations by CO_2 in the Venus thermosphere suggest that temperatures are as much as 40 K above the VIRA values in the region of the antisolar point. The effect of this different temperature distribution has been assessed by substituting the CO_2 and temperature profiles observed by Bertaux et al. on orbit 104 (near midnight) to the VIRA distribution. The shape and absolute values of the predicted intensity remains almost unaffected when the warmer distributions deduced from the SPICAV occultation are used.

[17] To document the question of the scale height, for each limb profile, we have determined the value of the apparent emission scale height H in the region extending between Z_p + 5 km and Z_p +15 km (except if the scale height varies rapidly in this altitude range), where Z_p is the altitude of the emission peak. The resulting distribution is shown in Figure 12. The distribution of H values covers more than an order of magnitude, ranging from about 2 to more than 30 km. If the homopause is located above the airglow peak region, as suggested by the determination of the homopause altitude from the Pioneer large probe descent, the airglow layer is in the homosphere dominated by eddy mixing. In these conditions, the analytical solution to equations (2) and (3) indicates that the topside scale height of the constituents flowing downward toward the chemical sink region varies as 1/K. With the altitude dependence adopted in our model, this implies that both the O and N densities vary as the square root of the CO_2 density. Consequently, since the airglow volume emission rate is proportional to the product of the O and N densities, the airglow scale height above the peak altitude is close to the value of the background atmosphere (mostly CO_2), which, according to the VIRA model, is on the order of 3.1 km at 0000 LT near the equator. Instead, if the emission is located above the homopause and controlled by molecular diffusion in the absence of wind, the airglow scale height is that of the geometric mean ~4.6 km of the O and N individual scale heights. Both values are indicated as vertical bars in Figure 12. The scale height determined from the analysis of the limb scans observed closer to the planet with PV-OUVS by *Gérard et al.* [1981] was ~3.2 km, in close agreement with the value expected for turbulent downward transport of the atoms. It is clear that a large fraction of the observations (over 90%) exhibit an apparent scale height in excess of this value. Most of these larger values are observational effects due to the combination of (1) a finite field of view of the instrument whose value depends on the spatial bin size used for a given observation, (2) the distance between the spacecraft and (3) the slit orientation relative to the planetary limb. As mentioned before, the projected aperture of the field of view on the limb ranges between 3 and 27 km, which tends to smooth the observed limb profile and to increase the apparent topside scale height.

[18] Figure 13 shows the O(^{3}P) and N(^{4}S) vertical distribution calculated from the best fit to the limb profile of orbit 320 in Figure 11. The maximum atomic oxygen density is predicted at 111 km where it reaches 4×10^{11} cm^{-3}. This value is in good agreement with the O density determined by *Drossart et al.* [2007] and *Gérard et al.* [2008] from the vertical distribution at the limb of the $O_2(^1\Delta)$ infrared airglow observed with the VIRTIS spectral imager. The atomic nitrogen density profile presents a peak of 2×10^8 cm^{-3} at 122 km. This result may be compared with the N density profiles calculated previously by *Stewart et al.* [1980] or by *Bougher et al.* [1990] for solar maximum activity at 2400 LT with the Venus TGCM and VIRA models and reported in their Figure 5. The calculated maximum N density was about 7×10^8 cm^{-3} at 112 km, in reasonably good agreement with the result of Figure 13, considering the different solar activity levels and local times. In Figure 11, two other simulations are compared with observed NO limb profiles. One (orbit 321, lat 53.8°N, LT = 0048) shows a peak at 105 km and is very well reproduced by the 1-D model both in magnitude and shape. The last one (orbit 324, lat 17.9°N, LT = 0118) presents a shallow peak at 119 km, while the best fit model produces maximum limb intensity at 112 km. The parameters of the fit for orbit 321 are $\phi_O = 6.6 \times 10^{10}$ cm^{-2} s^{-1}, $A = 4 \times 10^{12}$. For orbit 324, the parameters are $\phi_O = 8.2 \times 10^{10}$ cm^{-2} s^{-1}, and A = 0. In this latter case, downward transport solely by molecular diffusion alone is even slightly too strong to match the emission peak at 119 km. This result suggests that eddy diffusion may be locally quite weak or that upward

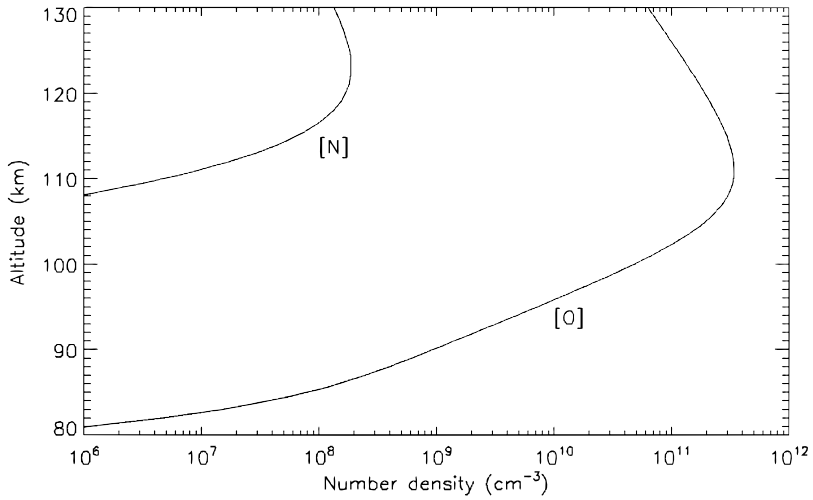

Figure 13. Vertical distribution of the atomic oxygen and nitrogen number density obtained from the model fitting the limb profile of orbit 320 shown in Figure 11.

vertical winds may act to raise the altitude of the airglow layer. The observed airglow topside scales heights are 13.3 km (orbit 320), 16 km (321) and 14.5 km (324). All three simulated profiles smoothed by the appropriate projected field of view exhibit an apparent scale height in agreement with the observed intensity drop above the emission peak. The modeled emission scale heights before smoothing are 3.6 km, 3.7 km and 4.6 km for orbits 320, 321 and 324, respectively. These values lie between the diffusive and the turbulent scale heights of 4.6 km and 3.1 km as discussed before.

5. Conclusions

[19] The NO nightglow emission is a good tracer of atmosphere dynamics in the Venus thermosphere. The nightside lower thermosphere of the planet remains relatively unexplored, especially the minor constituents densities and their dynamics. SPICAV observations of the NO nightglow provide a set of limb profiles data that have been used to analyze the NO vertical distribution in detail. From the comparison with a one-dimensional chemical-diffusive model, we have determined values for the eddy diffusion coefficient. The value of the A coefficient in formula (4) is 7.4×10^{11}, 4×10^{12} and 0 for the cases modeled in this study. The first two values are 0.09 to 0.5 smaller than the earlier determination based on NO airglow observations from Pioneer Venus. We note that the PV-OUVS limb observations were made at low latitudes near maximum solar activity. The profiles described here were obtained in the northern hemisphere, generally away from the bright spot reported by *Stewart et al.* [1980]. The nitrogen downward fluxes at 130 km range between 1×10^8 and 4×10^9 cm^{-2} s^{-1} with typical values of 2×10^9 cm^{-2} s^{-1}. The deduced O fluxes are less than the average column production rate of O atoms on the Venus dayside which was estimated at 8×10^{12} cm^{-2} s^{-1} by *Leu and Yung* [1987], in agreement with the discussion by *Gérard et al.* [2008]. Similarly, the daytime N average column production was found to be $\sim 1.3 \times 10^{10}$ atoms cm^{-2} s^{-1} by *Gérard et al.* [1988] at solar maximum and about 9×10^9 atoms cm^{-2} s^{-1} in the VTGCM photochemistry [*Bougher et al.*, 1990]. The N vertical fluxes on the nightside derived from these observations thus also appear compatible with the availability of N atoms on the dayside. We also find that the topside scale height of the NO airglow layer is in agreement with that expected for constituents in diffusive equilibrium or diffusing downward through the homosphere.

[20] One of the main results in the Venus Express observations is the large variability in the brightness of the NO nightglow emission. This feature was already apparent in the individual NO brightness maps obtained from PV-OUVS presented by *Stewart et al.* [1980] and in Figure 9 by *Bougher et al.* [1990]. It is not related to concurrent solar activity which remained very low throughout the period of these observations. It implies timescales as short as an Earth day or less. A similar variability is present in the O_2 ($^1\Delta$) emission arising from three-body recombination of O atoms at 1.27 μm that have been observed with VIRTIS-M, also on board Venus Express. Both limb and nadir observations [*Drossart et al.*, 2007; *Gérard et al.*, 2008; *Hueso et al.*, 2008; G. Piccioni et al., Molecular oxygen nightglow from the VIRTIS near IR observations in the Venus upper mesosphere, submitted to *Journal of Geophysical Research*, 2008] indicate that the brightness of the O_2 emission and its peak altitude exhibit substantial variations sometimes on timescales on the order of an hour or so. This variability may be caused by time variations in gravity waves breaking which potentially decelerate the SSAS flow.

[21] The SPICAV limb observations confirm and complete this picture and they also show the presence of strong horizontal gradients. Such gradients may be interpreted as signatures of localized regions of enhanced or decreased downward fluxes of atoms producing the patchy structure that had been observed on individual maps. In the southern hemisphere, the larger distance of the spacecraft from the planet precludes high-resolution limb observations. Therefore, the statistical bright spot near midnight slightly south of the equator was generally not captured in this tangential limb observing mode. It is thus not possible at this stage to

confirm whether the emission maximum is at the same location during solar minimum periods. If so, the comparison with the morphology of the O_2 ($^1\Delta$) emission due to three-body recombination of O atoms which has a peak near midnight near the equator would suggest that the zonal winds which shift the NO airglow at 113 km toward dawn have a different regime near 96 km. In any case, the features described in this study should be additional constraints to future three-dimensional models of the Venus nightside.

[22] **Acknowledgments.** The authors thank the SPICAV and the Venus Express teams for the excellent quality of their work. J.-C. Gérard is supported by the Belgian Fund for Scientific Research (FNRS). This research was funded by the PRODEX program of the European Space Agency (ESA) managed with the help of the Belgian Space Policy Office. The construction of the SPICAV instrument was funded by CNRS, CNES, and ESA/PRODEX.

References

Bertaux, J.-L., et al. (2005), Nightglow in the upper atmosphere of Mars and implications for atmospheric transport, *Science*, *307*, 566–569, doi:10.1126/science.1106957.

Bertaux, J.-L., et al. (2007a), SPICAV on Venus Express: Three spectrometers to study the global structure and composition of the Venus atmosphere, *Planet. Space Sci.*, *55*, 1673–1700, doi:10.1016/j.pss.2007.01.016.

Bertaux, J.-L., et al. (2007b), A warm layer in Venus' cryosphere and high altitude measurements of HF, HCl, H_2O and HDO, *Nature*, *450*, 646–649, doi:10.1038/nature05974.

Bougher, S. W., J. C. Gérard, A. I. F. Stewart, and C. G. Fesen (1990), The Venus nitric oxide night airglow: Model calculations based on the Venus Thermospheric General Circulation Model, *J. Geophys. Res.*, *95*, 6271–6284, doi:10.1029/JA095iA05p06271.

Bougher, S. W., S. Rafkin, and P. Drossart (2006), Dynamics of the Venus upper atmosphere: Outstanding problems and new constraints expected from Venus Express, *Planet. Space Sci.*, *54*, 1371–1380, doi:10.1016/j.pss.2006.04.023.

Campbell, I. M., and C. N. Gray (1973), Rate constants for the O (^{3}P) recombination and association with N (4S), *Chem. Phys. Lett.*, *18*, 607–609, doi:10.1016/0009-2614(73)80479-8.

Campbell, I. M., and B. A. Thrush (1966), Behaviour of carbon dioxide and nitrous oxide in active nitrogen, *Trans. Faraday Soc.*, *62*, 3366–3374, doi:10.1039/tf9666203366.

Cox, C., A. Saglam, J.-C. Gérard, J.-L. Bertaux, F. González-Galindo, F. Leblanc, and A. Reberac (2008), Distribution of the ultraviolet nitric oxide Martian night airglow: Observations from Mars Express and comparisons with a one-dimensional model, *J. Geophys. Res.*, doi:10.1029/2007JE003037, in press.

Dalgarno, A., J. F. Babb, and Y. Sun (1992), Radiative association in planetary atmospheres, *Planet. Space Sci.*, *40*, 243–246, doi:10.1016/0032-0633(92)90062-S.

Drossart, P., et al. (2007), Infrared spectral imaging observations of Venus by VIRTIS reveal a dynamical upper atmosphere, *Nature*, *450*, 641–645, doi:10.1038/nature06140.

Feldman, P. D., H. W. Moos, J. T. Clarke, and A. L. Lane (1979), Identification of the UV nightglow from Venus, *Nature*, *279*, 221–222, doi:10.1038/279221a0.

Fox, J. L. (1994), Rate coefficient for the reaction N + NO, *J. Geophys. Res.*, *99*, 6273–6276, doi:10.1029/93JA03299.

Gérard, J.-C., A. I. F. Stewart, and S. W. Bougher (1981), The altitude distribution of the Venus ultraviolet airglow and implications on vertical transport, *Geophys. Res. Lett.*, *8*, 633–636, doi:10.1029/GL008i006p00633.

Gérard, J.-C., E. J. Deneye, and M. Lerho (1988), Sources and distribution of odd nitrogen in the Venus daytime thermosphere, *Icarus*, *75*, 171–184, doi:10.1016/0019-1035(88)90135-2.

Gérard, J.-C., A. Saglam, G. Piccioni, P. Drossart, C. Cox, S. Erard, R. Hueso, and A. Sánchez-Lavega (2008), The distribution of the O_2 infrared nightglow observed with VIRTIS on board Venus Express, *Geophys. Res. Lett.*, *35*, L02207, doi:10.1029/2007GL032021.

Groth, W., D. Kley, and U. Schurath (1971), Rate constant for the infrared emission of the NO ($C^2\Pi \rightarrow A^2\Sigma^+$) transition, *J. Quant. Spectrosc. Radiat. Transfer*, *11*, 1475–1480, doi:10.1016/0022-4073(71)90109-9.

Hedin, A. E., H. B. Niemann, W. T. Kasprzak, and A. Seiff (1983), Global empirical model of the Venus thermosphere, *J. Geophys. Res.*, *88*, 73–83.

Hueso, R., A. Sánchez-Lavega, G. Piccioni, P. Drossart, J. C. Gérard, I. Khatuntsev, L. Zasova, and A. Migliorini (2008), Morphology and dynamics of Venus oxygen airglow, *J. Geophys. Res.*, *113*, E00B02, doi:10.1029/2008JE003081.

Leu, M.-T., and Y. L. Yung (1987), Determination of O_2 ($a^1\Delta_g$) and O_2 ($b^1\Sigma^+g$) yields in the reaction O + ClO → Cl + O_2: Implications for photochemistry in the atmosphere of Venus, *Geophys. Res. Lett.*, *14*(9), 949–952, doi:10.1029/GL014i009p00949.

Nair, H., M. Allen, A. D. Anbar, Y. L. Yung, and R. T. Clancy (1994), A photochemical model of the Martian atmosphere, *Icarus*, *111*, 124–150, doi:10.1006/icar.1994.1137.

Stewart, A. I., and C. A. Barth (1979), Ultraviolet night airglow of Venus, *Science*, *205*, 59–62, doi:10.1126/science.205.4401.59.

Stewart, A. I. F., J.-C. Gérard, D. W. Rusch, and S. W. Bougher (1980), Morphology of the Venus ultraviolet night airglow, *J. Geophys. Res.*, *85*, 7861–7870, doi:10.1029/JA085iA13p07861.

Svedhem, H., et al. (2007), Venus Express-The first European mission to Venus, *Planet. Space Sci.*, *55*, 1636–1652, doi:10.1016/j.pss.2007.01.013.

Titov, D. V., et al. (2006), Venus Express science planning, *Planet. Space Sci.*, *54*, 1279–1297, doi:10.1016/j.pss.2006.04.017.

von Zahn, U., K. H. Fricke, H. J. Hoffmann, and K. Pelka (1979), Venus: Eddy coefficients in the thermosphere and in the inferred helium content of the lower atmosphere, *Geophys. Res. Lett.*, *6*, 337–340, doi:10.1029/GL006i005p00337.

Yung, Y. L., and W. B. DeMore (1982), Photochemistry of the stratosphere of Venus: Implications for atmospheric evolution, *Icarus*, *51*, 199–247, doi:10.1016/0019-1035(82)90080-X.

J.-L. Bertaux, C. Nehmé, and E. Villard, Université de Versailles Saint-Quentin-UVSQ, Service d'Aéronomie du CNRS, Boite Post 3, F-91371 Verrières-le-Buisson, France.

C. Cox, J.-C. Gérard, and A. Saglam, Laboratoire de Physique Atmosphérique et Planétaire, Université de Liège, Bâtiment B5c, Allée de 6 Août, 17, B-4000 Liège, Belgium. (jc.gerard@ulg.ac.be)